

Original Research

# DSC analyses of static and dynamic precipitation of an Al–Mg–Si–Cu aluminum alloy

Manping Liu<sup>a,\*</sup>, Zhenjie Wu<sup>a</sup>, Rui Yang<sup>a</sup>, Jiangtao Wei<sup>a</sup>, Yingda Yu<sup>b</sup>, Pål C. Skaret<sup>b</sup>,  
Hans J. Roven<sup>b</sup>

<sup>a</sup>School of Materials Science and Engineering, Jiangsu Province Key Laboratory of Materials Tribology, Jiangsu University, Zhenjiang 212013, China

<sup>b</sup>Department of Materials Science and Engineering, Norwegian University of Science and Technology (NTNU), Trondheim 7491, Norway

Received 28 September 2014; accepted 7 January 2015

Available online 8 May 2015

## Abstract

In the present investigation, both static and dynamic precipitations of an Al–Mg–Si–Cu aluminum alloy after solid-solution treatment (SST) were comparatively analyzed using differential scanning calorimetry (DSC). Dynamic aging was performed in the SST alloy through equal channel angular pressing (ECAP) at different temperatures of room temperature, 110, 170, 191 and 300 °C. For comparison, static artificial aging was conducted in the SST alloy at 191 °C with two aging times of 4 and 10 h. The DSC analyses reveal that the dynamic precipitation has occurred in the ECAPed samples, while the activation energies associated with the strengthening precipitates in the dynamic samples are considerably higher than the energies in the SST and static aged samples. The higher activation energies are probably attributed to the smaller grains and higher dislocation density developed after ECAP. The results in the present investigation allow the prediction of the type of the dynamic precipitates to influence the strength of the ultrafine grained alloy during ECAP at various temperatures.

© 2015 Chinese Materials Research Society. Production and hosting by Elsevier B.V. This is an open access article under the CC BY-NC-ND license (<http://creativecommons.org/licenses/by-nc-nd/4.0/>).

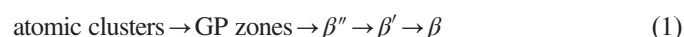
**Keywords:** Differential scanning calorimetry; Al–Mg–Si–Cu aluminum alloy; Dynamic aging; Precipitation behaviors; Equal channel angular pressing; Severe plastic deformation

## 1. Introduction

During the last two decades, severe plastic deformation (SPD) techniques have been widely applied to obtain ultrafine-grained (UFG) which can significantly improve the mechanical properties of Al–Mg–Si alloys [1,2]. Among various SPD techniques, equal channel angular pressing (ECAP) is the most promising method to fabricate large bulk UFG materials [3,4]. A significant increase of the strength is obtained during ECAP processing [5]. The precipitation behavior in ECAP processing microstructures is of great importance. The remarkable properties can be achieved directly after SPD. Differential scanning calorimetry (DSC) is used to study the precipitation sequence

in 6013 Al alloys. DSC is a powerful thermo-analytical technique for studying the thermodynamics and kinetics of phase changes [6].

Aluminum alloys of 6xxx series Al–Mg–Si having good formability, weld-ability and corrosion resistance [7,8] are extensively used in aerospace, vessel and automobile industries. Al–Mg–Si alloys can be strengthened by precipitation hardening. It is essential to study the precipitation sequence and precipitation behavior. The precipitation sequence in Al–Mg–Si alloy is:



where atomic clusters are the supersaturated solid solution; GP zones are generally spherical clusters with unknown structure [9,10];  $\beta''$  precipitates are fine needle shaped zones with monoclinic structure and are generally present in Al alloys aged to the maximum hardness;  $\beta'$  is rod shaped precipitates with hexagonal structure and are found in the overaged specimens;

\*Corresponding author.

E-mail addresses: [manping-liu@263.net](mailto:manping-liu@263.net),  
[manpingliu@ujs.edu.cn](mailto:manpingliu@ujs.edu.cn) (M.P. Liu).

Peer review under responsibility of Chinese Materials Research Society.

$\beta$  ( $Mg_2Si$ ) is an equilibrium phase in the precipitation sequence. Among these, the  $\beta''$  phases are considered to give the main contribution to strength. The significant improvement in strength of Al alloy upon SPD is due to the dynamic aging effect as reported in the earlier work. The strength and ductility of Al alloy were further improved by static aging [11]. Precipitation kinetics in aluminium alloys has been studied by using DSC. Kinetic parameters were investigated from the scan rate dependence of peaks observed in DSC curves [10]. Johnson–Mehl–Avrami (JMA) equation was used to calculate the activation energy for precipitation. Although the precipitation behavior in commercial Al–Mg–Si alloys has been reported in numerous works, much less information has been given on dynamic precipitation during ECAP [12].

In the present work, the precipitation behavior of static aging and dynamic aging samples has been investigated. The precipitation kinetics parameters during static aging and dynamic aging were obtained using DSC technique with the combination of JMA equation [13,14]. The precipitation kinetics during static aging and dynamic aging are compared with that in solid-solution treatment (SST) 6013 alloy.

## 2. Experimental

### 2.1. Materials and sample preparation

The original material investigated in the present work was commercially extruded 6013 Al–Mg–Si–Cu alloy rods with a diameter of 25 mm purchased from ALCOA in T6 peak-aged state. The composition of the alloy is given in Table 1. Square billets cut from the as-received rods along longitudinal axis were first solution-treated (SST) at 560 °C for 2 h, followed by quenching in water, then immediately processed by ECAP for four passes with route Bc (90° clockwise rotation around the sample axis between the pass). The ECAP die had a channel intersection angle  $\Phi=90^\circ$ , arc of curvature  $\Psi=20.6^\circ$  and the billet dimension was 19.5 mm × 19.5 mm × 100 mm. Dynamic aging was performed using the ECAP process at different temperatures of room temperature (RT), 110, 170, 191 and 300 °C. For comparison, static artificial aging was conducted in the alloy immediately after the solution heat treatment at 191 °C with two aging times of 4 and 10 h. Structural characterization of the ECAPed samples was performed by quantitative X-ray diffraction (XRD) with a D/max-2500PC diffractometer using Cu  $K\alpha$  radiation at 40 kV and 30 mA.

### 2.2. DSC measurements and JMA equation

To investigate the dynamic aging behaviors of the alloy during ECAP, all the SST, static and dynamic aged samples

Table 1  
Composition of the 6013 alloy (mass fraction, %).

Mg	Si	Cu	Mn	Fe	Zn	Ti	Cr	Al
0.8–1.2	0.6–1.0	0.6–1.1	0.2–0.8	≤0.5	≤0.25	≤0.1	≤0.1	Bal.

were subjected to DSC analyses. Specimens for the DSC analyses were cut from the bulk samples and cleaned with ultrasonic wave pool. The final mass of each DSC specimen was about 30 mg. The specimen for DSC testing was equilibrated at 20 °C and then heated to 500 °C with a heating rate of 10 °C per min under an argon atmosphere.

In the present investigation, JMA equation is used to calculate the activation energy for evolution of clusters and strengthening phases in the SST, static and dynamic aged samples. For non-isothermal transformation process [15], the modified JMA equation is given by:

$$f = 1 - \exp(-k_1^n t^n) \tag{2}$$

$$k_1 = k_0 \exp(-Q/RT) \tag{3}$$

where  $Q$  is the activation energy,  $T$  is absolute temperature,  $R$  is the gas constant,  $k_0$  is the constant, thus, the rate of transformation can be written as:

$$\frac{df}{dt} = k_1(T)F(f) \tag{4}$$

where  $F(f)$  is the implicit function of  $f$  from Eq. (2). Therefore, the following relation can be derived as the heating rate is 10 °C min<sup>-1</sup>:

$$\ln \left[ \frac{y(T)}{\int_{T_s}^{T_f} y(T)dT} \frac{1}{6} \frac{1}{1 - \int_{T_s}^T y(T)dT / \int_{T_s}^{T_f} y(T)dT} \right] = \ln k_0 - Q/RT \tag{5}$$

Apparently, a plot of  $\ln [(df/dT)(dT/dt)1/F(f)]$  vs  $1/T$  will give a straight line of slope from which the value of the activation energy can be obtained;  $k_0$  can be determined by the intercept.

## 3. Results

### 3.1. Microstructure

Fig. 1 shows the XRD peaks of the materials processed by ECAP at different temperatures. The structural parameters and dislocation density of the ECAPed alloy are shown in Table 2. The X-ray parameters demonstrate that the temperature of ECAP strongly influences the size of the investigated alloy.

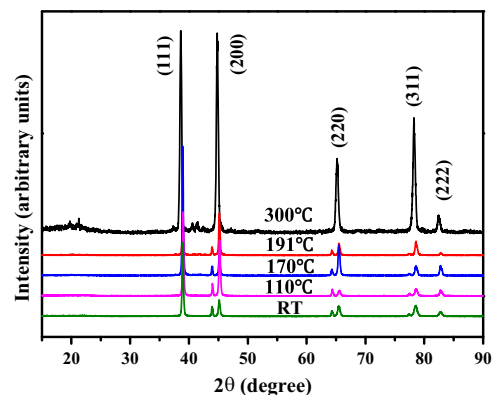


Fig. 1. XRD patterns of the alloy after ECAP at different temperatures.

Table 2

Structural parameters and dislocation density of 6013 alloy processed by ECAP.

State	$D_{\text{XRD}}$ (nm)	$\langle \epsilon^2 \rangle^{1/2}$ (%)	$\rho$ ( $10^{14} \text{ m}^{-2}$ )
SST+ECAPed at RT	66	0.092	1.70
SST+ECAPed at 110 °C	74	0.093	1.53
SST+ECAPed at 170 °C	112	0.111	1.20
SST+ECAPed at 191 °C	168	0.104	0.746
SST+ECAPed at 300 °C	–	0.017	0.275

The grain size ( $D_{\text{XRD}}$ ) increased tremendously from 66 nm to 168 nm as the temperature increased from RT to 191 °C (Table 2). The microstrain ( $\langle \epsilon^2 \rangle^{1/2}$ ) of the alloy processed by ECAP at 170 °C is larger than the others (Table 2). The values of grain size and microstrain were used to calculate the dislocation density in the ECAPed alloy by the equation given below [16,17]:

$$\rho = 2\sqrt{3} \frac{\langle \epsilon^2 \rangle^{1/2}}{D_{\text{XRD}}b} \quad (6)$$

where  $b=0.286$  nm is the magnitude of the Burgers vector. The calculated dislocation density of the ECAPed alloy is shown in Table 2. The dislocation density ( $\rho$ ) decreased significantly from 1.70 to  $0.275 \times 10^{14} \text{ m}^{-2}$  as the temperature increased from RT to 300 °C (Table 2). All above measurements indicate that the grain sizes, microstrains and dislocation densities of the ECAP alloy are strongly influenced by the temperature of process.

### 3.2. DSC analysis

Fig. 2 shows DSC thermograms of the SST and static aged specimens at 191 °C with different times. There are four exothermic peaks in the DSC thermogram of the Al–Mg–Si–Cu alloy in SST condition (curve A in Fig. 2), which are referred to as peak 1, peak 2, peak 3 and peak 4, respectively. Peak 1 was suggested to be caused by clusters of Si and Mg atoms. Peak 2 was supposed to be the result of formation of GP zones. Peak 3 and peak 4 were caused by the precipitation of  $\beta''$  and  $\beta'$ , respectively. These peaks observed in the SST alloy are similar to those published in the literature on similar alloys [18–22].

As seen from the thermograms of the static aged specimens (curves B and C in Fig. 2), no peaks corresponding to the formation of the clusters and GP zones are observed. The absence of these two low temperature peaks is attributed to the fact that the static aged specimens have no clusters/GP zones to form during DSC analysis. These results in these two static aged specimens indicate that the clustering reaction and the precipitation of GP zones had already been completed before DSC analysis. However, the exothermic peaks (peak 3 and peak 4) corresponding to the  $\beta''$  and  $\beta'$  still exist in both the static aged specimens (curves B and C in Fig. 2). In comparison with the curve A for the SST specimen, the intensity of these exothermic peaks has decreased and the

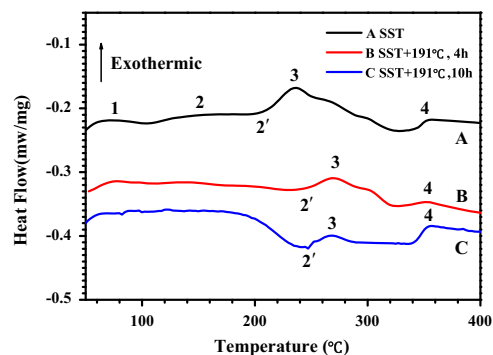


Fig. 2. DSC curves of the SST and static aged specimens at 191 °C with different times.

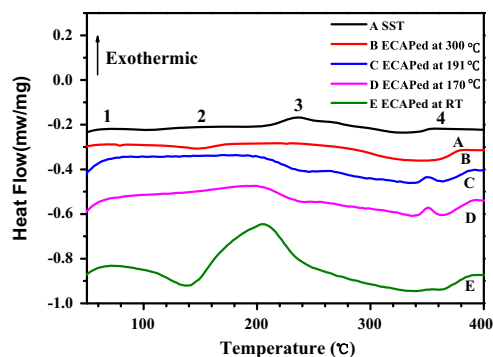


Fig. 3. DSC curves of the SST and dynamic aging specimens ECAPed at different temperatures.

position of the peak 3 corresponding to the strengthening phase  $\beta''$  in both conditions has shifted to higher temperatures about 270 °C from the temperature about 240 °C in the SST specimen. These observations suggest that the precipitation of  $\beta''$  phase in both the two static aged specimens has already taken place before the DSC analysis [23]. In addition, the endothermic peak 2 before exothermic peak  $\beta''$  have been observed in both curves B and C. Obviously, these endothermic peaks are the dissolution of the GP zones initially present in the base materials before DSC analysis. Therefore, it is reasonable to believe that the appearance of the peak 3 in both curves B and C mainly result from the dissolution of the GP zones. In other words, a considerable amount of  $\beta''$  precipitates had already existed in both the static aged specimens before the DSC analysis. This argument is further supported in our previous work [24] by the fact that two hardness peaks were observed in the above static aged specimens at 191 °C with aging times of 4 and 10 h, respectively.

As shown in Fig. 3, the DSC curve shape, number, position and intensity of the peaks of the dynamic aging specimens ECAPed at different temperatures are varied as compared with that of the peaks of the SST and static aged specimens. In the DSC thermogram of the ECAPed sample at RT (curve E in Fig. 3), peaks 3 and 4 are absent, indicating that a considerable amount of  $\beta''$  and  $\beta'$  have already taken place during dynamic aging. For the DSC thermogram of the ECAPed specimen at 170 °C (curve D in Fig. 3), the peak temperatures ( $T_p$ ) of the

first three exothermic peaks have moved to higher temperatures as compared to that of the similar peaks in the SST curve (curve A in Fig. 3). Another major difference observed with the DSC plots of SST material to ECAPed material at 170 °C is the fourth exothermic peak. The peak  $\beta''$  has been completely suppressed in ECAPed alloy. The peak accounting for the formation of  $\beta'$  precipitates now appear as a more narrow peak occurring at 306 °C. DSC thermogram of ECAPed sample at 191 °C shown in Fig. 3 is similar to the curve of ECAPed sample at 170 °C. DSC thermogram of ECAPed sample at 300 °C obtained with 10 °C min<sup>-1</sup> heating rate is shown in Fig. 3. By contrast, the first peak is missing from the curve, thereby showing that processing by ECAP gives a structure containing precipitates without the presence of Mg–Si clusters, indicating that a considerable amount of clustering had already taken place. The peak temperature of the GP zones has moved to high temperature. The peaks  $\beta''$  and  $\beta'$  are missing from the

DSC thermograms for the specimens by ECAP at 300 °C, indicating that the  $\beta''$  precipitation has already formed during the ECAP processing. This observation confirms that ECAP has a significant influence on the precipitation characteristics in these alloys. This also could be due to the high temperature during the ECAP processing. These indicate that ECAP processing has significantly affected the precipitation sequence during aging.

Table 3 shows peak temperatures ( $T_p$ ) of  $\beta''$  and  $\beta'$  in SST and static aged and dynamically aged DSC thermograms of the 6013 alloy. Compared with that of the SST material, the  $T_p$  of peak  $\beta''$  in static aging materials increase. The  $T_p$  of peak  $\beta'$  in both the static aging materials are similar to the  $T_p$  in SST material. In the material dynamically aged at RT, the  $\beta''$  and  $\beta'$  precipitates are missing. With increasing dynamic aging temperature, the  $T_p$  of peak  $\beta''$  increase and the  $T_p$  of peak  $\beta'$  decrease for the dynamically aged materials. In particular, peak  $\beta''$  and  $\beta'$  can no longer be observed when the dynamic aging temperature is 300 °C.

Table 3  
Peak temperatures of  $\beta''$  and  $\beta'$  on DSC thermograms after static and dynamic aging.

State	$T_p$ of peak $\beta''$ (°C)	$T_p$ of peak $\beta'$ (°C)
SST	237	357
SST+191 °C, 4 h	269	355
SST+191 °C, 10 h	267	357
SST+ECAPed at RT	–	–
SST+ECAPed at 170 °C	256	351
SST+ECAPed at 191 °C	261	349
SST+ECAPed at 300 °C	–	–

### 3.3. Activation energy

Fig. 4 shows the JMA plots for the various exothermic peaks in SST. In SST and dynamically aged material, peaks corresponding to Mg–Si cluster, GP zones,  $\beta''$  phase and  $\beta'$  phase were analyzed to calculate activation energy. The obtained activation energies from dynamically aged material were compared with its bulk SST material. Table 4 shows the obtained activation energies of various processed conditions.

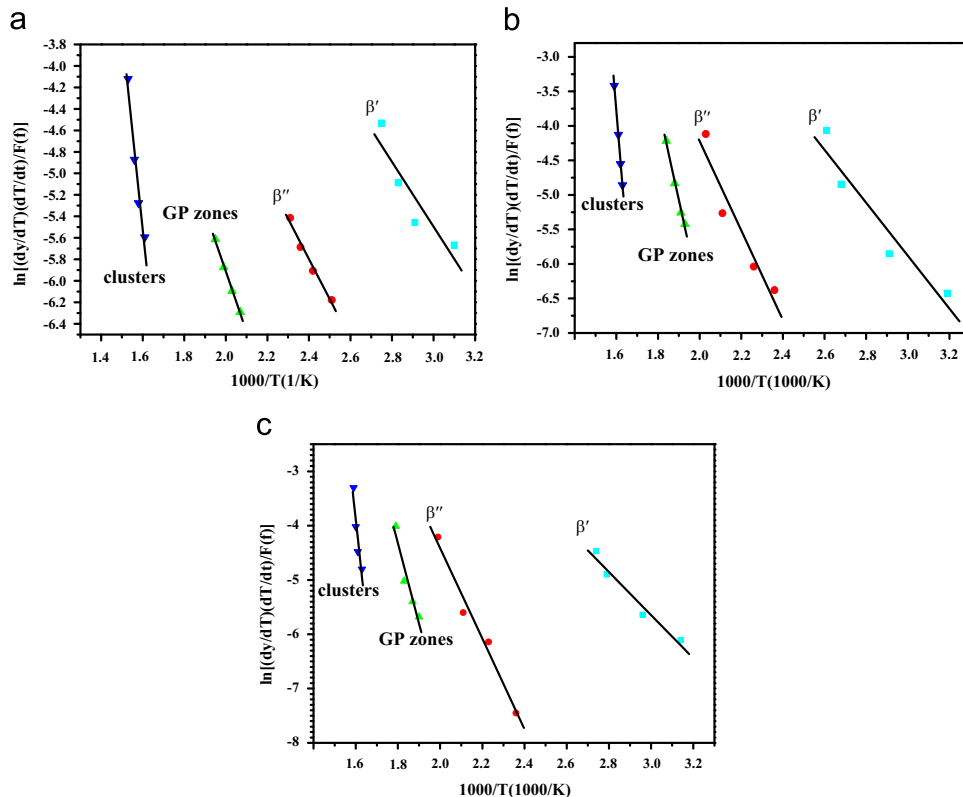


Fig. 4. JMA plots for the various exothermic peaks: (a) SST, (b) ECAPed at 170 °C, (c) ECAPed at 191 °C.

The values of activation energy obtained for cluster formation and GP zones in SST material are 25 kJ mol<sup>-1</sup> and 32 kJ mol<sup>-1</sup>, respectively. The activation energy value of GP zones is in good agreement with the value reported in other literature [25]. In dynamically aged material, the obtained activation energies for cluster formation and GP zone formation are higher than the values in SST material. In dynamically aged material, the dislocations can slow down the precipitate formation.

In SST material (Fig. 4a), the obtained activation energy for the β'' formation is 47 kJ mol<sup>-1</sup>. Vedani et al. have reported that the activation energy β'' formation in Al–Mg–Si alloy as 72 kJ mol<sup>-1</sup>, which is higher than the value observed in the present work [26]. This shows that there is no consistency in the reported literature. The obtained activation energy for the β' formation is 88 kJ mol<sup>-1</sup>. It is very close to those obtained by the reported value [26]. In the material dynamically aged at 170 °C, the activation energies obtained for the β'' formation and the β' formation are 118 kJ mol<sup>-1</sup> and 295 kJ mol<sup>-1</sup>, respectively. These values are much higher than those associated with β'' and β' formation in SST material. In the material dynamically aged at 191 °C, the activation energies obtained for the β'' formation and the β' formation are 122 kJ mol<sup>-1</sup> and 298 kJ mol<sup>-1</sup>, respectively, which are higher than the values in the material dynamically aged at 170 °C. It indicates that the temperature may have influence on the formation of β'' and β' precipitation during ECAP processing.

Fig. 5 shows the JMA plots for β'' and β' precipitation in static aging materials. The activation energies corresponding to β'' and β' precipitates are obtained and they are shown in Table 5. It is observed that the activation energies in static aging samples are higher than that in solution treated samples. The β'' precipitates and β' precipitates are difficult

to precipitate during DSC study, which increases the activation energies. The activation energies of the specimen aged at 191 °C for 4 h are lower as compared to that of the specimen aged at 191 °C for 10 h (Table 5). It indicates that the precipitates of the sample aged at 191 °C for 10 h are unstable during the following DSC study.

4. Discussion

From the DSC data, the activation energy values of dynamically aged 6013 alloy are higher than that of the SST alloy. It reveals that the formation of precipitates is really difficult in the following DSC testing. The close up view of the DSC thermograms is shown in Fig. 6. As shown in Fig. 6, the β'' precipitation peak clearly decreased in the ECAPed sample. It implies that most of the β'' has precipitated during the ECAP processing and the β'' precipitations were obviously decreased in the subsequent DSC study. Thus, it can be supposed that, the formation of β'' is promoted by ECAP [26]. In other words, dynamic precipitation has occurred in the ECAPed samples

Table 5  
Activation energies of precipitates in SST and static aging samples (kJ mol<sup>-1</sup>).

Type of precipitates	Solution treated	Static aging for 4 h	Static aging for 10 h
β''	47	142	135
β'	88	232	210

Table 4  
Activation energies of various processed conditions (kJ mol<sup>-1</sup>).

Type of precipitates	Solution treated	ECAP at 170 °C	ECAP at 191 °C
Mg–Si cluster	25	34	33
GP zones	32	57	69
β''	47	118	122
β'	88	295	298

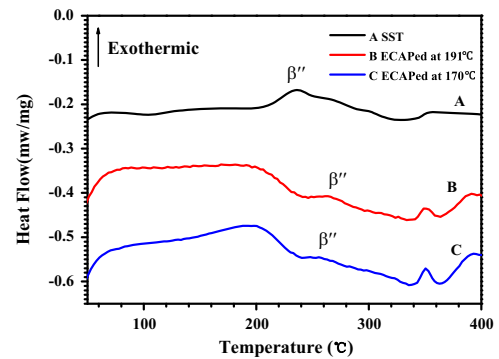


Fig. 6. DSC curves of the SST and dynamically aged 6013 alloy.

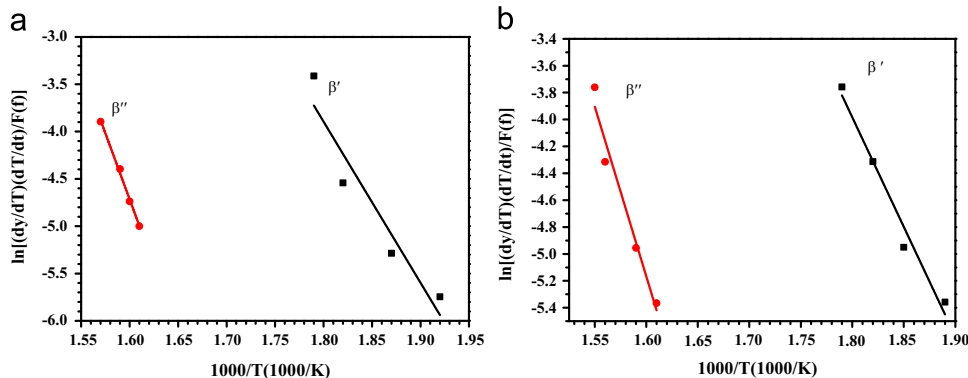


Fig. 5. JMA plots for the various exothermic peaks: (a) SST+191 °C, 4 h (b) SST+191 °C, 10 h.

before DSC analysis. In addition, the grain size decreased considerably and dislocation density increased in the ECAPed samples as shown in Table 2. As such, there are two possible reasons for the higher activation energies for the  $\beta''$  and  $\beta'$  participates in the dynamic samples. (i) The  $\beta''$  and  $\beta'$  participates have taken place during the ECAP processing, which make the precipitates difficult to produce during DSC testing. (ii) Deformation induced dislocations and boundaries have retarded the formation of  $\beta''$  and the  $\beta'$  [27]. Therefore, the higher activation energies are probably attributed to the smaller grains and higher dislocation density developed after ECAP.

## 5. Conclusions

- (1) The quantitative XRD analysis indicates that the grain sizes and dislocation densities of the ECAP alloy are strongly influenced by the temperature of the process. Average grain sizes measured by XRD are in the range 66–168 nm while the average dislocation density is in the range  $1.70 \times 10^{14}$ – $0.275 \times 10^{14} \text{ m}^{-2}$  in the deformed alloy.
- (2) As compared with the SST thermogram, no peaks corresponding to the formation of the clusters and GP zones are observed in the thermograms of the static aging materials. These results indicate that the clustering reaction and the precipitation of GP zones had already been completed in the two static aged specimens before DSC analysis.
- (3) In the DSC thermograms of the ECAPed samples at RT and 300 °C, peaks  $\beta''$  and  $\beta'$  are absent. For the DSC thermograms of the ECAPed specimen at 170 and 191 °C, peaks  $\beta''$  has been completely suppressed. These results confirm that the  $\beta''$  and  $\beta'$  precipitates have already taken place during dynamic aging. In other words, dynamic precipitation has occurred in the ECAPed samples before DSC analysis.
- (4) Based on the JMA analysis, the activation energies associated with the major exothermic peaks of the strengthening precipitates in the dynamic samples are considerably higher than the energies in the SST and static aged samples. The higher activation energies are probably attributed to the smaller grains and higher dislocation density developed after ECAP.
- (5) The results in the present investigation allow the prediction of the type of the dynamic precipitates that may influence the strength of the ultrafine grained alloy during ECAP at various temperatures.

## Acknowledgements

This work was supported by the Basic Research Program (Natural Science Foundation) of Jiangsu Province (grant

BK2012715), the Key University Science Research Project of Jiangsu Province (grant 14KJA430002), the Foundation of the Jiangsu Province Key Laboratory of High-end Structural Materials Project (grant hsm1301), and the National Natural Science Foundation of China (grant 50971087).

## References

- [1] G. Nurislamova, X. Sauvage, M. Murashkin, R. Islamgaliev, R. Valiev, *Philos. Mag. Lett.* 88 (2008) 459–466.
- [2] A.S. Khan, C.S. Meredith, *Int. J. Plast.* 26 (2010) 189–203.
- [3] Y. Huang, P.B. Prangnell, *Scr. Mater.* 56 (2007) 333–336.
- [4] B. Cherukuri, T.S. Nedkova, R. Srinivasan, *Mater. Sci. Eng., A* 410 (2005) 394–397.
- [5] K. Hockauf, L.W. Meyer, M. Hockauf, M. Hockauf, T. Halle, *J. Mater. Sci.* 45 (2010) 4754–4760.
- [6] P. Lang, T. Wojcik, E. Povoden-Karadeniz, A. Falahati, E. Kozeschnik, *J. Alloys Compd.* 609 (2014) 129–136.
- [7] W.J. Kim, J.Y. Wang, S.O. Choi, H.J. Choi, H.T. Sohn, *Mater. Sci. Eng., A* 520 (2009) 23–28.
- [8] X. Sauvage, M.Y. Murashkin, R.Z. Valiev, *Kovove Mater.* 49 (2011) 11–15.
- [9] S. Esmarili, X. Wang, D.J. Lloyd, *Metall. Mater. Trans. A* 34 (2003) 751–763.
- [10] S.K. Panigrahi, R. Jayaganthan, V. Pancholi, M. Gupta, *Mater. Chem. Phys.* 122 (2010) 188–193.
- [11] P.N. Rao, D. Singh, R. Jayaganthan, *J. Mater. Sci. Technol.* 30 (2014) 998–1005.
- [12] H.J. Roven, M.P. Liu, J.C. Werenskiold, *Mater. Sci. Eng., A* 483–484 (2008) 54–58.
- [13] K.S. Ghosh, K. Das, U.K. Chatterjee, *Metall. Mater. Trans. A* 38 (2007) 1965–1975.
- [14] X. Fang, M. Song, K. Li, *J. Min. Metall. B* 46 (2010) 171–180.
- [15] K.S. Ghosh, N. Gao, *Trans. Nonferrous Met. Soc. China* 21 (2011) 1199–1209.
- [16] R.Z. Valiev, M.Y. Murashkin, A.V. Ganeev, *Phys. Met. Metallogr.* 113 (2012) 1193–1201.
- [17] A.P. Zhilyaev, T.G. Langdon, *Prog. Mater. Sci.* 53 (2008) 893–979.
- [18] G.C. Weatherly, A. Perovic, N.K. Mukhopadhyay, D.J. Lloyd, D.D. Perovic, *Metall. Mater. Trans. A* 32 (2001) 213–218.
- [19] L. Zhen, S.B. Kang, *Mater. Lett.* 37 (1998) 349–353.
- [20] X. Wang, W.J. Poole, S. Esmaili, D.J. Lloyd, J.D. Embury, *Metall. Mater. Trans. A* 34 (2003) 2913–2924.
- [21] M.P. Liu, H.J. Roven, Y. Yu, J.C. Werenskiold, *Mater. Sci. Eng., A* 483 (2008) 59–63.
- [22] L.J. Hu, S.J. Zhao, *J. Mater. Sci.* 47 (2012) 6872–6881.
- [23] J. Buha, R.N. Lumley, A.G. Crosky, K. Hono, *Acta Mater.* 55 (2007) 3015–3024.
- [24] M.P. Liu, T.H. Jiang, J. Wang, Q. Liu, Z.J. Wu, Y.D. Yu, P.C. Skaret, H.J. Roven, *Trans. Nonferrous Met. Soc. China* 24 (2014) 3858–3865.
- [25] S. Esmaili, D.J. Lloyd, W.J. Poole, *Acta Mater.* 51 (2003) 3467–3481.
- [26] M. Vedani, G. Angella, P. Bassani, D. Ripamonti, A. Tuissi, *J. Therm. Anal. Calorim.* 87 (2007) 277–284.
- [27] P.N. Rao, B. Viswanadh, R. Jayaganthan, *Mater. Sci. Eng., A* 606 (2014) 1–10.